REVISION 1

Identification of nanocrystalline goethite in reduced clay formations. Application to the Callovian-Oxfordian formation of Bure (France)

Myriam Kars[1]*, Catherine Lerouge[2], Sylvain Grangeon[2], Charles Aubourg[1], Christophe Tournassat[2], Benoît Madé[3] and Francis Claret[2]

1 Laboratoire des Fluides Complexes et leurs Réservoirs, Université de Pau et des Pays de l'Adour, Avenue de l'Université, 64013 Pau cedex, France

2 BRGM, Environment and Process Division, 3, avenue Claude Guillemin, F-45060 Orléans Cedex 2, France

[3]Andra – Parc de la Croix Blanche, 1-7 rue Jean Monnet, 92298 Châtenay-Malabry Cedex, France

* now at : Center for Advanced Marine Core Research, Kochi University, B200 Monobe, Nankoku, 783-8502, Japan

Corresponding author: M. Kars, jm-mkars@kochi-u.ac.jp

ABSTRACT

The Callovian-Oxfordian (COx) clay formation in the Paris Basin (France) has been the target of many studies investigating the feasibility of deep nuclear waste disposal in a reduced clay formation. To determine the mobility of radionuclides in the host rock formation, modeling of the porewater chemistry, particularly iron solute concentrations, is necessary. Notably, this study aims to understand the supersaturation of Fe(III) oxyhydroxides given by models. Fe(III) oxyhydroxides have been identified magnetically in unpreserved Callovian-Oxfordian samples. In this study, a set of magnetic measurements are used to detect the Fe-bearing magnetic minerals present in the COx clay formation. A core sample from the borehole FOR1118, preserved from air since its collection, is the target of this study. The magnetic measurements performed show that magnetite and goethite are the main magnetic minerals (< 0.2%), together with probable greigite, and occur in low concentrations. Goethite occurs as nanoparticles dispersed in the clayey matrix, and not enclosed in other minerals or in organic matter. It is unlikely that the goethite is an alteration by-product, as particular care was undertaken. This finding resolves the discrepancies between observations and previous modeling results.

Keywords: goethite, nanoparticles, Callovian-Oxfordian clay formation, Paris Basin

Introduction

The Underground Research Laboratory (URL) built in the Callovian-Oxfordian Clay Formation (COx Clay) in Bure, France, is an experimental site used by the French National Radioactive Waste Management Agency (Andra) to test the feasibility of deep nuclear disposal in a reduced clay formation. To assess the durability of materials (e.g. glass, stainless steel, concrete, engineered clay barrier), and to determine the speciation and related mobility of the radionuclides in the host rock formation, it is necessary to model the chemistry of the clay porewater (e.g. Gaucher et al., 2009). Porewater composition models still have some deficiencies that need to be addressed. One of the most problematic issues is the understanding and modeling of iron (Fe) solute concentrations and the subsequent understanding of redox conditions in the formation. This information is mandatory for robust blind simulation modeling of redox perturbations in reduced clay formations (e.g. migration of redox sensitive radionuclides). For instance, predicted water compositions are supersaturated with respect to (Fe(III)) oxy(hydr)oxides (Gaucher et al., 2009). To date, all of the various microscopic and spectrometric techniques used on very well preserved samples of COx Clay in liquid nitrogen failed to predict the presence of Fe oxy(hydr)oxides (Tournassat et al., 2008; Lerouge et al., 2011). This inconsistency between observations and modeling could result from (1) a concentration of Fe(III) oxy(hydr)oxides which is too low to be detected by the different techniques or (2) a problem with the model.

This study aims to test the first hypothesis using a rock magnetic approach in order to detect the magnetic minerals (e.g. iron oxides, oxyhydroxides) possibly present in the reduced clay-rich formation. The main approach used in this paper is based on low-temperature magnetic measurements (from 10 to 400 K). It is non-destructive and allows the identification of magnetic

minerals, even if they occur in very low concentrations on the order of part per million per volume (ppmv) –part per billion per volume (ppbv).

Rock magnetism in Callovian-Oxfordian formation: a brief review

Diamagnetism is a property of all magnetizable minerals. However, diamagnetism is overshadowed if any other forms of magnetism are present (paramagnetism, ferromagnetism). When a mineral is subjected to a magnetic field (H), it acquires an induced magnetization, M, that is the sum of the transient and remanent magnetizations contributions. Only the ferromagnetic (sensu lato) minerals can retain a remanence. The magnetic susceptibility, χ=M/H, measured at room temperature under a weak magnetic field, is expressed as: $\chi = \chi_{dia} + \chi_{para} + \chi_{ferro}$. In argillaceous rocks, χ_{dia} is ~ -14 µSI (Hrouda, 1986). χ_{para} is similar to χ_{ferro}, depending on the ratio of clays (χ_{para}) and ferromagnetic minerals (χ_{ferro}). In the Callovian-Oxfordian Bure claystones, χ is dominated by the paramagnetic contribution (χ_{para}) and a positive correlation exists between the magnetic susceptibility and the amount of clays (Esteban, 2006 and references therein). The magnetic susceptibility values and the saturation remanence at room temperature are generally low (< 500 µSI and < 100 µAm² kg^{-1}, respectively) and indicate that a few ferromagnetic grains are present (e.g. Moreau et al., 2005; Esteban, 2006; Aubourg and Pozzi, 2010; Kars et al., 2012). In order to characterize the ferromagnetic contribution, remanence should be investigated.

Room temperature measurements are the most commonly used because they are faster and cheaper than the other techniques. An isothermal remanent magnetization (IRM) is monitored at room temperature with increasing applied magnetic field (generally up to 1-2 T) to achieve saturation. IRM acquisition and hysteresis loops indicate the minerals coercivities, but do not

allow discrimination between minerals with similar coercivity. Nevertheless, statistical analysis and modeling help to discriminate and quantify different IRM components (e.g. Heslop et al., 2002; Egli, 2004). Another way to distinguish mineral coercivities is to impart an IRM with increasing magnetic field values on the three axes, X, Y and Z. This will distinguish between low, medium and high coercivities, respectively (Lowrie, 1990). Then, IRM is thermally demagnetized up to 700°C (maximum temperature generally used). Recognition of the spectrum of unblocking temperature (T_{ub}) on a given axis will identify the magnetic mineral. Globally, magnetite is a low to medium coercive mineral ($T_{ub} \leq 580$°C), iron sulfides (greigite, pyrrhotite) are medium to high coercive minerals ($T_{ub} \leq 320$°C for pyrrhotite), and hematite ($T_{ub} \leq 670$°C) and goethite ($T_{ub} \leq 120$°C) are high coercive minerals. However, this presents some limitations. A recent study by Rochette et al. (2005) has shown that a very high magnetic field (up to 57 T) is necessary to saturate goethite. These high values cannot be reached by magnetometers classically used in rock magnetism laboratories. In addition, thermal demagnetization leads to chemical alteration of the magnetic minerals as a result of heating.

Finally, low-temperature (LT) magnetic measurements (from 300 down to 5 K) appear to be the best method, as they present many advantages. First, because the measurement is performed below room temperature, no sample alteration occurs. Second, similar to the thermal demagnetization, the magnetic minerals are recognized by their magnetic behavior below room temperature. Magnetite shows a magnetic transition at ~120 K, called the Verwey transition, which corresponds to a change in symmetry from cubic to monoclinic (e.g. Muxworthy and McClelland, 2000; Özdemir et al., 2002). Hematite shows a Morin transition at ~250 K corresponding to a spin reorientation in the C-axis (e.g. Özdemir et al., 2008). Goethite displays a remanence increase from room temperature during cooling, probably as a result of vacancy rearrangement (Dekkers, 1989). Maghemite also shows a remanence increase from room

113 temperature during cooling, but a smaller increase than that of goethite (generally 10%; Özdemir
114 and Dunlop, 2010). Pyrrhotite shows a magnetic transition at ~32-35 K called the Besnus
115 transition which probably corresponds to a change in symmetry from monoclinic to triclinic
116 (Dekkers et al., 1989; Rochette et al., 1990; Wolfers et al., 2011). This temperature range also
117 corresponds to the magnetic state transition from paramagnetism to antiferromagnetism of Fe-Mn
118 carbonates. Siderite ($FeCO_3$) and rhodochrosite ($MnCO_3$) transitions occurs at ~38 K and ~32 K,
119 respectively (Housen et al., 1996; Frederichs et al., 2003; Kosterov et al., 2006). The third
120 advantage is that these low-temperature magnetic measurements allow detection of magnetic
121 minerals at very low concentrations (~10^{-6} g g^{-1} – ppm to ~10^{-9} g g^{-1} – ppb).
122 Recent magnetic studies have been performed on COx claystones from different Andra boreholes
123 in the Paris Basin (Esteban, 2006; Esteban et al., 2006; Aubourg and Pozzi, 2010; Blaise et al.,
124 2013). Esteban et al. (2006) showed that the magnetic susceptibility increases downhole
125 depending on the lithology. The summit of the Callovian-Oxfordian (COx) formation is of lower
126 susceptibility because it is more clay-depleted. The maximum clay zone, located at the middle of
127 the Callovian-Oxfordian formation presents the highest susceptibility values, and rather low
128 remanence. This is due to a high concentration of iron-bearing clay minerals, and low
129 concentrations of ferromagnetic minerals. The base of the COx formation presents high low field
130 magnetic susceptibility values and displays the highest remanence. In these boreholes,
131 occurrences of iron oxides [(titano)-maghemite or magnetite] and iron sulfides (pyrrhotite,
132 greigite, pyrite) have been documented (Esteban et al., 2006). Aubourg and Pozzi (2010) also
133 showed the presence of goethite (probably nanometer-sized) based on LT magnetic
134 measurements on samples from EST211 borehole. This 2010 study is, to the best of the authors'
135 knowledge, the first to show the occurrence of Fe(III)-bearing oxy-hydroxides in the COx clay
136 formation. The origin of goethite was, however, not discussed. It remains plausible that this

mineral is present due to oxidation through contact with the atmosphere, as no particular care was taken for sample preservation. This present study differs from that of Aubourg and Pozzi (2010) by the analyses of very well preserved COx claystones. The oxidation effect was also tested.

Materials

In this study, Callovian-Oxfordian claystones from the Paris Basin (France) are analyzed (Table 1). An additional goethite (α-FeOOH) sample from a laterite of New Caledonia was also measured in order to compare its magnetic behavior to the bulk magnetic signature of COx claystones. The selected goethite was separated by handpicking under binocular.

Callovian-Oxfordian Claystones

General mineralogy of the claystones. Callovian-Oxfordian (COx) claystones from the Underground Research Laboratory (URL) site in Bure (France) (Gaucher et al., 2004; Andra, 2005; Clauer et al., 2007; Lerouge et al., 2011) were extensively studied for their chemistry and mineralogy. COx Clay had undergone limited burial (600 m) and diagenetic (T < 50°C) processes (Pellenard et al., 1999; Elion et al., 2005; Clauer et al., 2007). Its mineralogy consists of a dominant clay fraction (> 40 %) associated with carbonates (< 25 %) and quartz (< 25 %), with minor K-feldspars (< 2 %) (Tournassat et al., 2007; Table 2). Clay minerals are dominantly illite-smectite mixed-layer minerals, illite, chlorite and kaolinite with minor glauconite, muscovite and biotite (Pellenard et al., 1999; Gaucher et al., 2004; Pellenard and Deconinck, 2006). A maximum clay zone (MCZ) is defined at 486-489 m depth in the borehole EST-205. Beneath and within this

MCZ, the clay fraction is high (40-60 %) and illite-smectite mixed-layer minerals are ordered following a Rechweite parameter (junction probability) of 1 (ISR1). Illite-smectite mixed-layer minerals are dominantly illitic in the whole formation, and in addition to the disappearance of discrete smectite with increasing burial depth, the transition from a random (R0) to a R1 stacking mode may be driven by interaction with organic matter (Claret et al., 2004). Above the MCZ, the clay fraction decreases towards the top in favor of a silty, then a calcareous-rich, fraction (Gaucher et al., 2004; Andra, 2005). Kaolinite and biotite disappear, and the ordered illite-smectite mixed-layer minerals (ISR1) are replaced by randomly interstratified illite-smectite mixed-layer minerals dominated by smectite (ISR0). Chlorite is tri-octahedral, iron-rich, and of the chamosite-type, according to the Hey classification (Hey, 1954; Lerouge et al., 2011).

The carbonate fraction is composed predominantly of calcite, with minor dolomite, ankerite and siderite. Accessory phases (< 2 %) are pyrite, rutile/anatase, celestite, and apatite. Organic matter content is low (< 0.6 %), and immature in the petroleum sense. Amongst all the mineral phases, the main Fe carrier phases are, in order of decreasing iron content, pyrite, glauconite, biotite, chlorite, muscovite, and illite/illite-smectite mixed layers (Tournassat et al., 2008; Lerouge et al., 2011).

Studied claystones. Two core samples (EST26479 and K119), deemed to be representative of the COx Clay Formation, were selected for this study. Sample EST26479 is a preserved core sample from the FOR1118 borehole collected at depth -124.06 m (Z_{NGF}; NGF: Nivellement Général de la France) in 2009. The sample was cleaned and conditioned under nitrogen gas in a gas cell on the field immediately after drilling. It was then transferred and kept into a glove box in a nitrogen atmosphere (O_2 concentration lower than or equal to 1 ppm) (modified from

Gaucher et al., 2009). Sample K119 is an unpreserved core sample of the EST-205 borehole collected at depth -111.50 m (Z_{NGF}) in 2000 and always kept in open atmosphere. Both samples belong to the C2b1 sub-unit and are almost close to the gallery level. Their mineralogical composition is summarized in Table 2.

In order to determine if pyrite and organic matter contain enclosed magnetic minerals (e.g. iron oxides), they were separated from the claystone argillaceous matrix by handpicking. Two samples were considered (Table 1). A pluri-cm–scale pyritized ammonite collected in 2008 during the opening of a new gallery in the Bure URL was selected to obtain a representative fraction of pyrite associated with minor amounts of organic matter. An organic matter-rich fraction was separated by handpicking in the preserved EST26479 sample.

Sample preparation for low temperature measurements

The selected massive goethite, non-preserved from atmosphere, was first crushed into ~1 mm-sized grains and washed three times with 95 % alcohol in an ultrasonic bath (5 minutes). It was then dried at 40 °C, before being measured in this present study.

The preserved EST26479 bulk sample was crushed in two different ways: into coarse granulates and fine-grained powder. Coarse granulates and a first aliquot of fine-grained powder were prepared and inserted in two gelatin capsules in the glove box under nitrogen atmosphere. They were then encapsulated and sealed in a glass vial prior to removing it from the glove box. Glass vials were opened just before the magnetic measurement. Another aliquot of fine-grained powder was prepared in air 24 hours before the measurement in order to test the oxidation effect after 24 hours.

The pyrite sample used for magnetic measurements was obtained by crushing the pluri-cm–scale pyritized ammonite from a gallery opened in 2008 at the Bure URL, and its inner part was selected. The sample was broken into mm-sized grains in air and rapidly wedged inside the gelatin capsule with quartz wool just before the measurement, in order to obtain fresh surfaces and to limit, as much as possible, sample oxidation.

The unpreserved K119 bulk sample and organic matter extracted from sample EST26479 were encapsulated in air just before measurement.

Methods

Raman spectrometry

Micro-Raman measurements were performed at BRGM with a Renishaw InVIA Reflex micro-spectrometer coupled to a DMLM Leica microscope equipped with 4 objectives with x5, x20, x50 and x100 magnification. The excitation laser was an argon laser (λ_0 = 514.5 nm). Each spectrum was acquired by two signal accumulations with an acquisition time of 10 seconds per analysis, over a spectral range which depends on the mineral studied. Calibration was done using the 520.4 cm^{-1} line of silicon. Instrument control and Raman measurements were performed with Renishaw WIRE^{TM} software.

Magnetic measurements

Low-temperature measurements. In order to determine the rock magnetic properties of the samples, low-temperature magnetic measurements were performed using SQUID cryogenic

230 magnetometers called Magnetic Properties Measurement System (MPMS) at the Institut de
231 Physique du Globe de Paris, France and at the Institute for Rock Magnetism, University of
232 Minnesota, USA. For this study, the evolution of a saturation isothermal remanent magnetization
233 (SIRM) obtained with the application of a 2.5 T magnetic field at room temperature (RT-SIRM at
234 300 K) was monitored. Though the term "saturation" is used, it should be noted that it is not a
235 true SIRM, as neither all goethite nor hematite will be saturated at 2.5 T. Two measurement
236 sequences, hereafter referred to as A and B, were used and are described below (see also
237 supplementary material).
238 Sequence A consists of a cooling/warming cycle of a SIRM imparted at room temperature, for
239 which the value at 300 K is named M1, from 300 K to 10 K. The sample was cooled down to 10
240 K and then warmed to 300 K in zero magnetic field (trapped field < 0.1 μT). This 300-10-300 K
241 sequence was used to determine the nature, and an approximated crystal size, of the magnetic
242 minerals present in the samples.
243 Sequence B is designed specifically to underline goethite and to quantify its abundance. This
244 sequence is based on Guyodo's et al. (2006) protocol. Before applying sequence B, the sample
245 was primarily measured with sequence A. Then at 300 K, it was warmed to 395 K, above the
246 Néel temperature of goethite which is ~393 K (120°C; Özdemir and Dunlop, 1996). At this
247 temperature, the remanence carried by goethite is lost, as goethite becomes paramagnetic. At 395
248 K, the sample was cooled down to room temperature in a 2.5 T magnetic field. It is generally
249 designed to impart magnetization on a wide range of grain size of hard coercive minerals, i.e.,
250 maximize the amount of magnetization carried by goethite. At 300 K, the magnetic field was
251 switched off. The remanence at this temperature step is called M2. Then the sample underwent a
252 second cycle of cooling and warming from 300 K to 10 K and from 10 K to 400 K, similar to
253 sequence A. At 400 K, all the remanence carried by goethite was removed. Finally, a 400-10-300

K cycle ended the sequence. The two last cycles were performed in zero magnetic field. At the end of sequence B, the obtained remanent magnetization is referred to as M3. The difference between M2 and M3 is a proxy of the goethite concentration in the sample, as M2 is believed to concentrate all goethite and M3 is free of goethite (Guyodo et al., 2006). The approach used here differs from the Guyodo's et al. (2006) protocol by the non application of AF demagnetization at 200 mT after the measurement of M2 to remove the contribution of ferrimagnetic minerals with coercivity lower than 200 mT (e.g. magnetite). The sequence used in this study was designed to enhance the signal carried by goethite without removing the sample from inside the MPMS and to counterbalance the absence of a strong demagnetizer similar to the one used by Guyodo et al. (2006).

Finally, a third sequence was used on a COx sample and involved imparting an IRM at 10 K, called LT-SIRM, with a 2.5 T magnetic field. The sample was then warmed up to room temperature in zero magnetic field.

Magnetic measurements were performed on about 300-700 mg of sample (fragments or powder) wedged inside 0.5 x 1.4 cm gelatin capsules.

Room and high temperature measurements. To complete low-temperature magnetic measurements, room and high temperature measurements were also performed on the FOR1118 sample. Several aliquots were used. For the thermal demagnetization experiment, the FOR1118 samples were conditioned in plaster with a cylindrical shape. An IRM was imparted, by using an impulse magnetizer ASC IM-10-30, on the X, Y, Z axes with 0.08 T, 1.2 T and 2.8 T magnetic fields, corresponding to soft, medium and hard components, respectively (Lowrie, 1990). The specimens were then thermally demagnetized from 80°C to 600°C in an oven in the shielded room of the paleomagnetic laboratory of Université de Montpellier 2, in order to determine the

Curie/Néel temperature of the magnetic minerals present. The remanence was measured after each heating step with a 2G SQUID cryogenic magnetometer. One hysteresis loop with a 400 mT saturation field was measured with a Princeton Vibrating Sample Magnetometer at room temperature at the Institute for Rock Magnetism.

Results

Goethite

Goethite was measured with sequence B. The remanence values M1, M2, M3 are reported in Table A2 of the supplementary material.

The data show that the goethite remanence acquired at room temperature (M1 ~ 8.10^{-3} Am² kg^{-1}) increases about four times as temperature was reduced down to 10 K (Figure 1a). This magnetic behavior, associated with a high percentage increase, is typical of goethite according to the literature (e.g. Dekkers, 1989). When warming back to 300 K, the remanence shows characteristic quasi-reversible behavior. After the 300-395 K heating-cooling phase under a 2.5 T magnetic field (Figure 1a), the imparted SIRM at room temperature (M2 ~ 3.10^{-2} Am² kg^{-1}) was about four times higher than M1. The heating-cooling step under the magnetic field is then very useful to mobilize the goethite grains. From 300 to 395 K, the remanence decreases by 95 % when passing through the Néel temperature of goethite (120°C-393 K; Özdemir and Dunlop, 1996). When performing a 400-10-300 K cycle, the remanence shows an almost flat (constant) reversible behavior. All the goethite grains are thus demagnetized. About 15 % of the remanence (M3 ~ 1.10^{-3} Am^2 kg^{-1}) is nevertheless still present, suggesting that one or more magnetic phases with Curie/Néel temperature higher than 395 K occur (e.g. hematite) (Guyodo et al., 2006).

302 **Callovian-Oxfordian claystones from the Paris Basin**

303

304 **Bulk samples.** The room temperature hysteresis loop shows that the contribution of
305 ferromagnetics (sensu lato) is very small (Figure 2a). Saturation is reached at 400 mT suggesting
306 that the occurrence of low coercive minerals (magnetite or maghemite) (Figure 2b).
307 This is supported by the thermal demagnetization of IRMs showing that most of the remanence is
308 carried by the X axis (low coercive phase) (Figure 3). The drop in remanence at ~250 °C suggests
309 the presence of iron sulfides (greigite) (Roberts et al., 2011). Remanence is totally removed by
310 580 °C, indicating that magnetite is present. In specimen 2, a drop of the remanent magnetization
311 is observed at ~120 °C on the soft component (Figure 3). This drop could correspond to the
312 removal of a viscous component. No clear drop is identified on specimen 1 (Figure 3).
313 To better characterize the magnetic mineralogy of the COx claystones, additional measurements
314 were performed. Preserved fragments of EST26479 are measured at low temperature. The
315 remanence evolution through a cooling-warming cycle in zero magnetic field (sequence A)
316 shows that the remanence increases by ~30 % from 300 to 10 K, suggesting the occurrence of
317 goethite (Dekkers, 1989). The remanence drop of the Verwey transition of magnetite is not
318 recovered when warming back to room temperature (Figure 4a) (Muxworthy and McClelland,
319 2000; Özdemir et al., 2002).
320 In order to corroborate this preliminary result, a crushed EST26479 specimen is measured with
321 the sequences A and B. The cooling-warming SIRM cycles before and after the 395 K heating
322 phase under a 2.5 T field are quasi-superimposed (Figures 4b and4c). From 300 to 10 K, the
323 remanence increases by ~30 %, suggesting goethite. When warming back to room temperature,
324 the curves are reversible. After heating the sample to 395 K in zero magnetic field, ~76 % of the
325 EST26479 remanence remains. In other words, the fourth of the remanence is lost when heating

the sample to the Néel temperature of goethite (Özdemir and Dunlop, 1996). The fact that a non-negligible part of the remanence remains at the end of sequence B (after heating) suggests that one or more magnetic phases are present in the EST26479 sample in addition to goethite. These additional magnetic phase(s) have Néel/Curie temperatures higher than 400 K, such as (titano)-magnetite, maghemite or hematite. Neither the Verwey transition of magnetite nor the Morin transition of hematite is, however, observed on low-temperature measurements (Figures 4b and 4c).

Nevertheless, maghemite may be present in a minor amount. Maghemite and goethite are both magnetic minerals that could result from the oxidation of reduced iron-bearing phases. Oxidation is tested by considering two distinct COx samples. One EST26479 specimen left in air during 24 h after crushing is measured at low temperature (Figure 4d). The remanence regularly increases by ~46 % down to 10 K, typical of goethite. The cooling-warming cycle is reversible. The second sample came from the K119 borehole, and was left in air since its collection in 2000 (Figure 4e). The results obtained are similar to the 24h air EST26479 samples. For 24h air EST26479 and K119 claystones, no other magnetic minerals are identified with low-temperature magnetic measurements. Both analyzed samples thus show a ~50 % increase in remanence from 300 to 10 K, typical of goethite. This is higher than the ~30 % increase for the preserved samples (Figures 4a, 4b, 4c).

Pyrite and organic matter separates. Pyrite and organic matter are present in small amounts in the Callovian-Oxfordian clay formation (<1%) (Table 2; Gaucher et al., 2004). However, they represent a significant reduced-iron-rich fraction, which could be rapidly oxidized under oxic conditions to produce goethite. Measuring an SIRM on the pyrite-rich separate from a preserved pyritized ammonite (Figures 5a and 5b) was not possible because of the very low concentration

(or absence) of ferromagnetic minerals capable of retaining a remanence. Micro Raman spectra on pyrite fragments do not allow identification of any iron oxides or hydroxides (Figure 5c).

An organic matter-rich separate (with probable pyrite content) from the EST26479 sample was analyzed (Figures 5d and 5e). No evolution of the SIRM imparted at room temperature is observed when cooling down to 10 K (Figure 6). The warming curve shows irreversible behavior from ~60 K. This could suggest the presence of a magnetic phase. Neither magnetic transitions nor any particular SIRM increase during warming is identified. This means that magnetite, hematite and goethite can be excluded. Then, remaining candidates could be oxidized magnetite or maghemite. Based on the study by Esteban et al. (2006), maghemite is likely, although oxidized magnetite cannot be ruled out in the absence of complementary data.

Discussion

Similar to previous studies (Esteban et al., 2006; Aubourg and Pozzi, 2010; Blaise et al., 2013), magnetite is identified in preserved COx claystones when monitoring artificial remanence at low temperature (Verwey transition at 120 K, i.e. -153 °C) (Figure 4a) and at high temperature (T_{ub} < 580 °C) (Figure 3). Some magnetite grains might possibly be newly-formed during diagenesis. In the high temperature experiment, a break-in-slope near 250 °C suggests the presence of iron sulfides (Figure 3). Such behavior was also reported by Esteban (2006). In practice, it could be greigite or pyrrhotite. However, low-temperature experiments did not show evidence for the Besnus transition of pyrrhotite (at ~32 K) (Figures 4a, 4b). Thus, the iron sulfide is probably greigite. This mineral is a classic product of early diagenesis (Roberts et al., 2011). It is worth noting that the magnetic assemblage of both magnetite and greigite is expected to be representative of immature claystones according to Aubourg et al. (2012).

374

375 The low-temperature magnetic analysis revealed the diagnostic signature of goethite contribution
376 with an increase of remanence from 30% in preserved claystones to 50% in claystones
377 unpreserved from the atmosphere during cooling (Figure 4). It remains possible that a portion of
378 this increase in remanence from 300 K to 10 K is due to the contribution from maghemite. In any
379 case, goethite is observed in preserved COx claystones. Similar goethite signatures have been
380 reported by Aubourg and Pozzi (2010) and Blaise et al. (2013). By contrast, high-temperature
381 analysis failed in the firm identification of goethite in preserved COx claystones. A slight drop at
382 120°C is observed when demagnetizing the soft component of IRM (Figure 3) but it is unlikely
383 that this is due to goethite because this mineral has a hard coercivity (Rochette et al., 2005).
384 Therefore, this present study confirms that high-temperature techniques in rock magnetism are
385 not adapted to detect goethite contribution, but low-temperature (< 300 K) measurements appear
386 very useful.

387

388 Other magnetic phases are, however, probably present, but have not been clearly identified by
389 magnetic measurements. Maghemite as an accessory phase could not be dismissed, as pyrite and
390 organic matter extracts may show the occurrence of maghemite (Figure 6). The theoretically
391 well-marked Morin transition of hematite (~250 K; Özdemir et al., 2008) is not observed in the
392 studied samples. In addition, the high temperature measurements performed in this study do not
393 allow the recognition of hematite (Figure 3).
394 The different magnetic analyses conducted in this study provide evidence that goethite, magnetite
395 and possibly greigite are the main magnetic minerals in the COx samples which were carefully
396 preserved from any oxidation effects.

397

398 **Contribution of goethite in claystones**

399

400 The relative concentration, *c*, of goethite (with size above the blocking volume, Vb) in COx
401 claystones could be approximated by $c \sim$ (M2-M3)/Mrs with Mrs representing the saturation
402 remanent magnetization of goethite (Mrs = 0.05 $Am^2 kg^{-1}$; e.g. Dunlop and Özdemir, 1997). M2
403 is the IRM value at 300 K after the 2.5 T cooling phase between 400 and 300 K. M3 is the IRM
404 value at 300 K after the 300-400 K heating/cooling phase in a null magnetic field. In this
405 equation, only goethite is assumed to contribute to the measured SIRM. For the EST26479 COx
406 sample (Figure 4b), M2 is $1.58.10^{-4}$ $Am^2 kg^{-1}$ and M3 is $1.21.10^{-4}$ $Am^2 kg^{-1}$ (Table 3). The
407 estimated goethite concentration is then < 0.1 % of the mass. Similarly, a simplified calculation
408 of the goethite concentration, *c*, might be used for samples which were measured only with
409 sequence A. This is expressed as $c \sim$ M1/Mrs. For the preserved EST26479 fragments (Figure
410 4a), the estimated concentration is < 0.2 % (similar to the K119 sample). Magnetite and other
411 magnetic minerals might also occur. The Mrs of soft magnetite is ~10 $Am^2 kg^{-1}$ (Maher and
412 Thompson, 1999), i.e., 200 times higher than that of goethite, leading to an overestimation of the
413 goethite (above Vb) concentration. Such low concentration values explain why goethite has not
414 been identified before in the routine mineralogical analyses at room temperature. For instance, X-
415 ray diffraction has a threshold value of about 1 % when the mineralogical assemblage is complex,
416 as it is the case in clay-rich rocks, and detection is further complicated when phases are
417 nanocrystalline, because the intensity diffracted at each lattice point is distributed over a large
418 angular range.
419 However, the concentration of goethite occurring in sizes below Vb (superparamagnetic grains)
420 may be higher. The monitoring of the LT-SIRM of a preserved EST26479 sample displays a
421 significant decrease of ~60 % from 10 to 50 K (Figure 7). This suggests the presence of small

422 particles that unblock very rapidly (i.e. nanoparticles). These small particles could be magnetite,
423 goethite or other nano-magnetic minerals (greigite, maghemite). In addition to their low
424 concentrations in COx samples, the magnetic minerals occur in small sizes. Both features
425 together make them hardly detectable.
426
427 Finally, magnetic measurements carried out on both pyrite and organic matter extracts have
428 shown that they carry a small remanence. Iron oxides such as magnetite and maghemite, and iron
429 sulfides (greigite) can be evoked to explain the magnetic behavior observed in Figure 6. Based on
430 the available data, none of these can be ruled out. Magnetite and/or maghemite are more likely as
431 an alteration by-product because pyrite oxidizes into iron oxides. These iron oxides can also be
432 present as impurities resulting from the separation protocol, or impurities enclosed in pyrite and
433 organic matter. The measurements performed in this study do not permit the distinction between
434 these different hypotheses, and their origin is still debated. No goethite is identified in these two
435 extracts, suggesting that goethite is dispersed within the clayey matrix, rather than being locally
436 enriched as impurities or being consecutive oxidation by-products.
437
438 **Implications for the modeling of pore water chemistry in reduced clay formations**
439
440 The finding of small amounts of goethite and magnetite in COx samples preserved from
441 atmosphere are important for our understanding of the redox conditions which can be found in
442 the pore water of clay-rocks. Amongst pore water chemistry parameters, redox potential is one of
443 the most important because predictions of the solubility and the mobility of redox sensitive
444 species (e.g. uranium) rely on the accuracy of its determination. To date, it is difficult, if not
445 impossible, to measure directly the redox potential of the pore water in a clay-rocks sample. The

446 measurement of the redox potential of seepage water flowing from the clay formation to an
447 equipped borehole is subject to experimental artifacts: biological activity, including sulfate
448 reducing bacteria metabolism, has been always detected in such conditions (Vinsot et al., 2008).
449 This biological activity is not expected in-situ where the pore space is too limited for bacteria to
450 be active. Consequently, modeling the redox potential of the pore water is the only way to
451 estimate it, and the presence of goethite and magnetite in the mineralogical assemblage is an
452 important modeling constraint.
453 A comprehensive description of the modeling procedure that has been applied to the Callovian-
454 Oxfordian formation can be found elsewhere (Gaucher et al., 2009). The modeling procedure is
455 based on the finding of chemical controls that constrain the system at equilibrium following
456 Gibbs' Phase Rule. In pore water modeling, the concentrations of the solid phases are not
457 important, only the presence (or absence) of a phase at equilibrium provide useful constraints.
458 Sulfate is present in the pore water of Callovian-Oxfordian claystone and its concentration is well
459 constrained by measurements (Vinsot et al., 2008). Its concentration in solution is also in
460 agreement with equilibrium with celestite ($SrSO_4$). Redox potential can be calculated by
461 considering the S(VI)/S(-II) redox couple, provided that the concentration of S(-II) can be
462 estimated. Unfortunately, the S(-II) concentration cannot be measured and, if so, it is likely to be
463 subject to bacterial activity perturbation. If equilibrium with pyrite, that is in contact with the
464 pore water, is assumed, it is possible to estimate the S(VI)/S(-II) redox balance. Again, this is
465 only possible if the Fe(II) concentration is known. This is achieved by assuming equilibrium of
466 the pore water with siderite ($FeCO_3$), all other pore water parameters being controlled by other
467 constraints (e.g. equilibrium with calcite, quartz etc.). Applying this modeling procedure has led
468 to pore water compositions that are over-saturated with respect to goethite and other Fe(III)
469 (hydr-) oxides (Gaucher et al., 2009) where these phases had not been observed until now on

well-preserved samples, using, for instance, XRD and 77 K Mössbauer spectrometry (Tournassat et al., 2008). So far, two main explanations have been put forward to explain this inconsistency: (i) an inaccuracy in the Fe phases' solubility products as tabulated in the used database and (ii) an inaccuracy originating from the deviation of the composition of the actual iron carbonate phase from that of the pure siderite considered in the modeling approach (Gaucher et al., 2009, Pearson et al., 2011). A third explanation could be that pyrite and sulfate are not at equilibrium. Sulfate species are known not to be reduced easily at low temperatures through abiotic processes (Truche et al., 2010). This study brings a part of the answer. Magnetite and especially goethite (Fe(III)-bearing mineral) have been identified in the COx samples. Following this finding, a new pore water modeling has been conducted (Table 3) using the same mineral solubility database as the one used by, and available in, Gaucher et al. (2009).

Table 3 shows that considering different combinations of Fe/redox controlling phases has little effect on the modeled pH values which span a range of values from 7 to 7.5. The redox potential values (expressed here as pe = 0.059 Eh) are not much affected by the different hypotheses, with the exception of the goethite/siderite and goethite/magnetite calculation cases. For the three other systems, pH/pe couple values correspond to a single O_2 or H_2 fugacity value (an increase of one pH unit leads to a decrease of one pe unit). Table 3 shows also that all Fe phases identified in the formation cannot be at equilibrium with the pore water but this is a logical result of the direct application of a model following Gibbs' Phase Rule: the number of controlling phases in the system cannot exceed the number of degrees of freedoms in those calculations (see Pearson et al., 2011). Even so, the finding of two phases at near-equilibrium could indicate that these two phases can co-exist from a thermodynamics point of view. Here, it is apparently not the case: the co-existence of goethite and magnetite at equilibrium would lead to pyrite oversaturation but also to a Fe solute concentration that is not in agreement with the range of values measured in the

seepage waters from the formation (15 ± 11 µmol L^{-1} according to Gaucher et al., 2009). This result could indicate that one of the minerals goethite or magnetite is metastable in the investigated samples, or that the considered solubility products are not sufficiently accurate to draw any definitive conclusion. Indeed, the present study shows that goethite must be a nano-crystalline phase in the investigated samples. If so, its solubility might deviate from the value tabulated in databases that are representative of well-crystallized minerals. The solubility of goethite in our sample might therefore be larger than the tabulated value in the database (Electronic Appendix 1 in Gaucher et al. 2009). The line in Table 3 corresponding to the system magnetite/pyrite shows that a slight change in goethite solubility could be sufficient to achieve equilibrium between magnetite/goethite and pyrite. Moreover, for this calculation, the Fe concentration is consistent with the range of values measured in seepage water (Gaucher et al., 2009) and the siderite saturation index is only slightly negative (Table 3). This siderite under-saturation can be linked to the exact nature of the Fe carbonate: a sideroplesite whose solubility might be lower than the solubility of pure siderite (Tournassat et al. 2008, Lerouge et al., 2013). It is thus possible to reconcile the observations made in this study (i.e. the presence of nanocrystalline goethite and magnetite in pristine samples) with the pore water modeling results. A window of pH/redox conditions ranging from pH 7 to 7.5 and pe from -3 to -3.9 can be also given for the Fe(II)/Fe(III) redox controlling system.

Conclusive Remarks

Porewater modeling in Callovian-Oxfordian claystones from the Paris basin has predicted the occurrence of goethite; however, to date, standard observations on fresh or well-preserved samples have failed to detect it. In this study, the low-temperature magnetic properties of

518 isothermal remanent magnetization are used to detect trace amounts of goethite. Nanoparticles of
519 goethite, in addition to magnetite and possibly greigite, are detected in both preserved and
520 unpreserved claystones. This strengthens the idea that goethite is naturally present in COx
521 claystones and is not the result of oxidation in contact with atmosphere. This goethite is not
522 detected in pyrite and organic matter extracts. Goethite is probably dispersed within the clay
523 fraction. The low-temperature magnetic technique appears to be appropriate to detect
524 nanoparticles of goethite in sediments.
525
526
527 **Acknowledgments**
528 This research has been financially supported by the ANDRA-BRGM scientific partnership
529 (THERMOAR project). We are grateful to Dr. France Lagroix from the Institut de Physique du
530 Globe de Paris (IPGP) for her help during our stays and for fruitful discussions. Data from
531 Figures 1, 4 and 6 were obtained by using the MPMS from IPGP. The MPMS XL5Evercool used
532 was financed by the Conseil Régional d'Ile de France (No. I-06-206/R), INSU-CNRS, IPGP and
533 ANR. We would like also to thank the Institute for Rock Magnetism, University of Minnesota,
534 Minneapolis, USA and the Université de Montpellier 2, France for their instrumental facilities.
535 Nontronites samples were kindly provided by Hélène Gailhanou and Jebril Hadi from BRGM.
536 This paper benefited from the constructive reviews of Dr. Simo Spassov and an anonymous
537 reviewer. We would like to thank Dr. Joshua Feinberg for editorial handling.

538 **REFERENCES**

539

540 Andra (2005) Evaluation de la faisabilité du stockage géologique en formation argileuse, Dossier
541 2005. Collection Les Rapports.

542

543 Aubourg, C. and Pozzi, J-P. (2010) Toward a new < 250°C pyrrhotite-magnetite geothermometer
544 for claystones, Earth and Planetary Science Letters, 294(1-2), 47-57.

545

546 Aubourg, C., Pozzi, J-P. and Kars, M. (2012) Burial, claystones remagnetization and some
547 consequences to magnetostratigraphy, In: Remagnetization and chemical alteration of
548 sedimentary rocks, R.D. Elmore, A.R. Muxworthy, M.M. Aldana and M. Mena (eds), Geological
549 Society, London, Special Publication, 371, 181-188

550

551 Blaise, T., Barbarand, J., Kars, M., Ploquin, F., Aubourg, C., Brigaud, B., Cathelineau, M., El
552 Albani, A., Gautheron, C., Izart, A., Janots, D., Michels, R., Pagel, M., Pozzi, J-P., Boiron, M-C.,
553 and Landrein, P. (2013) Reconstruction of low temperature (< 100°C) burial in sedimentary
554 basins: a comparison of geothermometer sensibility in the intracontinental Paris Basin, Marine
555 and Petroleum Geology, http://dx.doi.org/10.1016/j.marpetgeo.2013.08.019

556

557 Claret, F., Sakharov, B. A., Drits, V.A., Velde, B., Meunier, A., Griffault, L., and Lanson, B.
558 (2004) Clay minerals in the Meuse-Haute Marne underground laboratory (France): possible
559 influence of organic matter on clay mineral evolution, Clays and Clay Minerals, 52(5), 515-532.

560

561 Clauer, N., Fourcade, S., Cathelineau, M., Girard, J-P., and Vincent, B. (2007) A review of
562 studies on the diagenetic evolution of the Dogger-to-Tithonian sedimentary sequence in the
563 eastern Paris Basin – impact on the physical and chemical rock properties. Mémoire de la Société
564 Géologique de France, 178, 59–71.
565
566 Dekkers, M.J. (1989) Magnetic properties of natural goethite II. TRM behaviour during thermal
567 and alternating field demagnetization and low-temperature treatment, Geophysical Journal
568 International, 97, 341-355.
569
570 Dekkers, M.J., Mattéi, J-L., Fillion, G., and Rochette, P. (1989) Grain-size dependence of the
571 magnetic behavior of pyrrhotite during its low-temperature transition at 34 K, Geophysical
572 Research Letters, 16(8), 855-858.
573
574 Dunlop, D., and Özdemir, Ö. (1997) *Rock magnetism: fundamentals and frontiers,* Cambridge
575 University Press, 573 pp.
576
577 Egli, R. (2004) Characterization of individual rock magnetic components by analysis of
578 remanence curves, 1. Unmixing natural sediments, Studia Geophysica et Geodaetica, 48, 391-
579 446.
580
581 Esteban, L. (2006) Anisotropies magnétique et de porosité des argilites du Callovo-Oxfordien du
582 laboratoire souterrain de l'Andra (Meuse/Haute-Marne, Bassin de Paris), PhD. Thesis, Université
583 Toulouse III – Paul Sabatier, 305 pp.
584

585 Esteban, L., Bouchez, J-L., and Trouillier, A. (2006) The Callovo-Oxfordian argillites from the
586 eastern Paris Basin: magnetic data and petrofabrics, Comptes Rendus Géoscience, 338, 867-881.
587
588 Frederichs, T., von Dobeneck, T., Bleil, U., and Dekkers, M.J. (2003) Towards the identification
589 of siderite, rhodochrosite and vivianite in sediments by their low-temperature magnetic
590 properties, Physics and Chemistry of the Earth, 28, 669-679.
591
592 Gaucher, E., Robelin, C, Matray, J.M., Négrel, G., Gros, Y., Heitz, J.F., Vinsot, A., Rebours, H. ,
593 Cassagnabère, A., and Bouchet, A. (2004) ANDRA underground research laboratory:
594 interpretation of the mineralogical and geochemical data acquired in the Callovo-Oxfordian
595 formation by investigative drilling, Physics and Chemistry of the Earth, 29, 55-77.
596
597 Gaucher, E.C., Tournassat, C., Pearson, F.J., Blanc, P., Crouzet, C., Lerouge, C., Altmann, S.
598 (2009) A robust model of pore-water chemistry of clayrock, Geochimica et Cosmochimica Acta,
599 73(21), 6470-6487.
600
601 Guyodo, Y., La Para, T.M., Anschutz, A.J., Penn, R.L., Banerjee, S.K., Geiss, C.E., and Zanner,
602 W. (2006) Rock magnetic, chemical and bacterial community analysis of a modern soil from
603 Nebraska, Earth and Planetary Science Letters, 251, 168-178.
604
605 Heslop, D., Dekkers, M.J., Kruiver, P.P., and van Oorschot, I.H.M. (2002) Analysis of isothermal
606 remanent magnetization acquisition curves using the expectation-maximization algorithm,
607 Geophysical Journal International, 148, 58-64.
608

609 Hey, M.H. (1954) A new review of the chlorites. Mineralogical Magazine, 30, 277–292.

610

611 Housen, B.A., Banerjee, S.K., and Moskowitz, B.M. (1996) Low-temperature magnetic
612 properties of siderite and magnetite in marine sediments, Geophysical Research Letters, 23(20),
613 2843-2846.

614

615 Kars, M., Aubourg, C., Pozzi, J-P., and Janots, D. (2012) Continuous production of nanosized
616 magnetite through low grade burial, Geochemistry Geophysics Geosystems, 13(8), Q08Z48,
617 doi:10.1029/2012GC004104.

618

619 Kosterov, A., Frederichs T., and von Dobeneck, T. (2006) Low-temperature magnetic properties
620 of rhodochrosite (MnCO3), Physics of the Earth and Planetary Interiors, 154, 234-242.

621

622 Lerouge, C., Vinsot, A., Grangeon, S., Wille, G., Flehoc, C., Gailhanou, H., Gaucher, E.C.,
623 Madé, B., Altmann, S. and Tournassat, C. (2013) Controls of Ca/Mg/Fe activity ratios in pore
624 water chemistry models of the Callovian-Oxfordian Clay Formation, Procedia Earth and
625 Planetary Science, 7, 475-478.

626

627 Lerouge, C., Grangeon, S., Gaucher, E.C., Tournassat, C., Agrinier, P., Guerrot, C., Widory, D.,
628 Fléhoc, C., Wille, G., Ramboz, C., Vinsot, A., and Buschaert, S. (2011) Mineralogical and
629 isotopic record of biotic and abiotic diagenesis of the Callovian-Oxfordian clayey formation of
630 Bure (France), Geochimica et Cosmochimica Acta, 75(10), 2633-2663.

631

632 Lowrie, W. (1990) Identification of ferromagnetic minerals in a rock by coercivity and
633 unblocking temperature properties, Geophysical Research Letters, 17(2), 159-162.
634
635 Maher, B.A., and Thompson, R. (1999) *Quaternary Climates, Environments and Magnetism,*
636 Cambridge: Cambridge University Press, 1-48.
637
638 Moreau, M-G., Ader, M., and Enkin, R.J. (2005) The magnetization of clay-rich rocks in
639 sedimentary basins: low-temperature experimental formation of magnetic carriers in natural
640 samples, Earth and Planetary Science Letters, 230, 193-210.
641
642 Muxworthy, A.R., and McClelland, E. (2000) Review of the low-temperature magnetic properties
643 of magnetite from a rock magnetic perspective, Geophysical Journal International, v. 140, p. 101-
644 114.
645
646 Özdemir, Ö., and Dunlop, D. (1996) Thermoremanence and Néel temperature of goethite,
647 Geophysical Research Letters, 23(9), 921-924.
648
649 Özdemir, Ö., Dunlop, D., and Moskowitz, B. (2002) Changes in remanence, coercivity, and
650 domain state at low temperature in magnetite, Earth and Planetary Science Letters, 194, 343-358.
651
652 Özdemir, Ö., Dunlop, D., and Berquó, T. (2008) Morin transition in hematite: size dependence
653 and thermal hysteresis, Geochemistry Geophysics Geosystems, 9(10), Q10Z01, doi:
654 10.1029\2008GC002110.
655

656 Özdemir, Ö., and Dunlop, D. (2010) Hallmarks of maghemitization in low-temperature
657 remanence cycling of partially oxidized magnetite nanoparticles, Journal of Geophysical
658 Research, 115(B02101), doi:10.1029/2009JB006756.
659
660 Pearson, F.J., Tournassat, C., and Gaucher, E.C. (2011) Biogeochemical processes in a clay
661 formation in situ experiment: Part E – Equilibrium controls on chemistry of pore water from the
662 Opalinus Clay, Mont Terri, Underground Research Laboratory, Switzerland, Applied
663 Geochemistry, 26, 990-1008.
664
665 Pellenard, P., Deconninck, J.F., Marchand, D., Thierry, J., Fortwrengler, D., and Vigneron, G.
666 (1999) Contrôle géodynamique de la sédimentation argileuse du Callovien–Oxfordien moyen
667 dans l'est du Bassin de Paris: influence eustatique et volcanique. Compte-Rendus de l'Académie
668 des Sciences Série IIA 328, 807–813.
669
670 Pellenard, P., and Deconinck, J.F. (2006) Mineralogical variability of Callovo-Oxfordian clays
671 from the Paris Basin and the Subalpine Basin. Compte-rendus Geosciences, 338, 854–866.
672
673 Roberts, A.P., Chang, L., Rowan, C.J., Horng, C.S., and Florindo, F. (2011) Magnetic properties
674 of sedimentary greigite (Fe_3S_4): an update, Review of Geophysics, RG1002,
675 doi:10.1029/2010RG000336.
676
677 Rochette, P. (1987) Magnetic susceptibility of the rock matrix related to magnetic fabric studies,
678 Journal of Structural Geology, 9(8), 1015-1020.
679

Rochette, P., Fillion, G., Mattéi, J-L., and Dekkers, M.J. (1990) Magnetic transition at 30-34 Kelvin in pyrrhotite: insight into a widespread occurrence of this mineral in rocks, Earth and Planetary Science Letters, 98, 319-328.

Rochette, P., Mathé, P.E., Esteban, L., Rakoto, H., Bouchez, J-L., Liu, Q., and Torrent, J. (2005) Non saturation of the defect moment of goethite and fine-grained hematite up to 57 T, Geophysical Research Letters, 32, L22309, doi: 10.1029/2005GL024196.

Tournassat, C., Gailhanou, H., Crouzet, C., Braibant, G., Gautier, A., Lassin, A., Blanc, P., and Gaucher, E.C. (2007) Two cation exchange models for direct and inverse modeling of solution major cation composition in equilibrium with illite surfaces, Geochemica et Cosmochimica Acta, 71, 1098-1114.

Tournassat, C., Lerouge, C., Blanc, P., Brendlé, J., Greneche, J-M., Touzelet, S., and Gaucher, E.C. (2008) Cation exchanged Fe(II) and Sr compared to other divalent cations (Ca, Mg) in the Bure Callovian-Oxfordian formation: implications for porewater composition modeling, Applied Geochemistry, 23(4), 641-654.

Truche, L., Berger, G., Destrigneville, C., Guillaume, D., and Giffaut, E. (2010) Kinetics of pyrite to pyrrhotite reduction by hydrogen in calcite buffered solutions between 90 and 180 °C: implications for nuclear waste disposal, Geochimica et Cosmochimica Acta, 74, 2894–2914

Vinsot A, Mettler, S., and Wechner, S. (2008) In situ characterization of the Callovo-Oxfordian pore water composition, Physics and Chemistry of the Earth A/B/C; 33, S75-S86.

Wolfers, P., Fillion, G., Ouladdiaf, B., Balou, R., and Rochette, P. (2011) The pyrrhotite 32K magnetic transition, Solid State Phenomena, 170, 174-179.

FIGURES CAPTIONS

Figure 1: Evolution of the RT-SIRM for the reference goethite during three successive cooling-warming cycles. (b) is a zoom of (a) in the 200-360 K temperature range. The increase in remanence from 300 to 10 K is 75 and 73% for cycles 1 and 2. A slight Morin transition of hematite is observed at ~250 K. Note that the remanence is almost entirely removed after the last heating step at 395 K (cycle 3).

Figure 2: a) Uncorrected and b) corrected hysteresis loop at room temperature for bulk Callovian-Oxfordian claystone from FOR1118. Note the high paramagnetic contribution in the sample. Hysteresis loop was corrected by assuming saturation above 70% of Hmax. Saturation is reached at 400 mT.

Figure 3: Thermal demagnetization of IRM showing soft, medium and hard components. Note that more than 50% of the initial remanence is lost by 250°C suggesting the presence of ferromagnetic iron sulfides (IS). All the remanence is lost at~580°C corresponding to the Curie temperature of magnetite (Mg). In specimen 2, a decrease in remanence is observed at ~120°C. This could correspond to the Néel temperature of goethite (G) or could be due to the removal of a viscous component.

Figure 4: a) Evolution of the RT-SIRM during a cooling-warming cycle of preserved COx fragments from FOR1118. The increase in remanence during cooling is due to the presence of goethite (G%=25). Note the presence of the Verwey transition of magnetite that is not recovered upon warming. b,c) Evolution of the RT-SIRM on three successive cooling-warming cycles for

732 powdered FOR1118 COx claystone (b: first cooling-warming cycle, c: second and third cycles)
733 after the heating phase at 395 K under a 2.5 T field. The increase in remanence during cooling
734 between 300 and 10 K is 30, 30 and 25% respectively. d, e) Evolution of the RT-SIRM during a
735 cooling-warming cycle for two unpreserved COx samples. The increase from 300 to 10 K is 46
736 and 50% for d) FOR1118 sample left for 24h in air after crushing and e) K119 (unpreserved since
737 its collection) respectively.
738
739 **Figure 5**: a) Macroscopic aspect of centimeter-sized pyriteous ammonite from the ANDRA URL
740 gallery; b) Backscattered electron image of framboidal pyrite; c) Example of Raman spectrum
741 acquired on pyriteous ammonite providing evidence of pyrite and excluding iron oxyhydroxide;
742 d) Macroscopic view of organic matter-rich ammonite fossil in the Callovian-Oxfordian clay
743 EST26479 core sample from the FOR1118 borehole – unpreserved sample; e) Backscattered
744 electron image of a pyriteous ammonite from the same sample – unpreserved sample.
745
746 **Figure 6**: Evolution of the RT-SIRM during a cooling-warming cycle for a pyrite+organic matter
747 extract. The irreversibility of the curve upon warming may indicate maghemite occurrence.
748
749 **Figure 7**: Evolution of the LT-SIRM of FOR1118 COx sample upon warming to 300 K. LT-
750 SIRM decreases by 60% from 10 to 50 K, indicating significant amount of small particles.
751
752

753 **APPENDIX**

754 See supplementary material.

755

756 **TABLES**

757

Sample name	Type	Location	Formation/ Age	Collection date	Preservation
EST26479	Claystones (fragments)	FOR1118 (-124.06 m)	C2b1 (COx)	2009	Preserved
EST26479	Claystones (powder)	FOR1118 (-124.06 m)	C2b1 (COx)	2009	Preserved
EST26479	Claystones (powder)	FOR1118 (-124.06 m)	C2b1 (COx)	2009	Unpreserved (24h air)
K119	Claystones (powder)	EST205 (-111.50 m)	C2b1 (COx)	2000	Unpreserved
Py1	Pyrite (powder)	Bure URL gallery (ammonite)	COx	2008	Unpreserved
OM1	OM + pyrite (tr.) (powder)	FOR1118 (-124.06 m)	COx	2009	unpreserved

758 Table 1: List of the samples from the Callovian-Oxfordian formation in the Paris Basin analyzed

759 in this study.

760

761

Mineral Phases		Abundance (% mass)	
		K119[a]	EST26479[b]
Carbonates	Calcite	13	20
	Ankerite	6	0
	Dolomite	6	4
	Siderite	0	2
	Total	**25**	**24**
Silicates	Quartz	21	19
	K-feldspar	4	tr.
	Plagioclase	2	tr.
	Total	**27**	**19**
Phyllosilicates	Illite + Illite/smectite	43	54
	Chlorite	2	1
	Biotite	tr.	tr.
	Kaolinite		
	Total	**45**	**55**
Others	Pyrite	1.7	tr.
	Rutile/anatase	1.4	0
	Celestite	0.7	0
Total Organic Carbon (TOC)		0.7	0.6

[a] After Tournassat et al. (2007).

[b] Determined from modeling of XRD patterns and chemical data, following the same procedure than that of K119.

762 Table 2: Mineralogical phases and total organic carbon present in the two Callovian-Oxfordian
763 claystones studied in this paper.

764

765

Systems	pH	pe	Fe (µmol L^{-1})	SI Goethite	SI Magnetite	SI Pyrite	SI Siderite
Siderite/pyrite	7.22	-3.0	47	1.0	0.9	0.0	0.0
Goethite/pyrite	7.51	-3.4	2	0.0	-2.0	0.0	-1.4
Magnetite/pyrite	7.31	-3.1	17	0.7	0.0	0.0	-0.4
Goethite/siderite	7.18	-3.9	47	0.0	-1.2	13.3	0.0
Goethite/magnetite	7.00	-3.9	149	0.0	-1.0	15.0	0.3

766 Table 3: Calculation of pH, pe, Fe concentrations and Fe phases saturation indices (SI) according
767 to the model and the database from Gaucher et al. (2009) and to four different hypotheses on the
768 Fe concentration and redox controls.

769

770

771

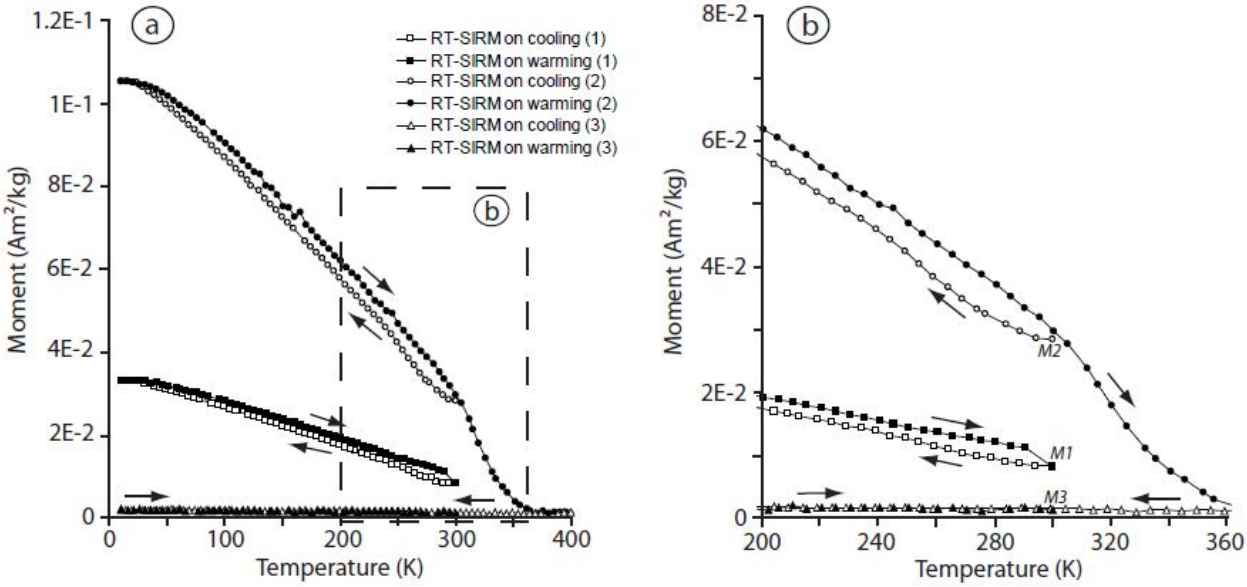

772

773 Figure 1

774

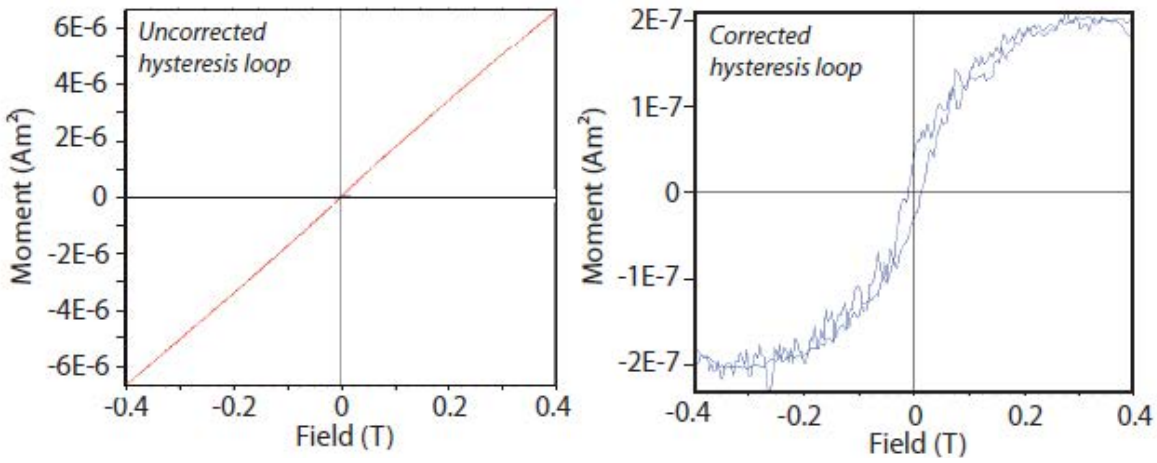

775

776 Figure 2

777

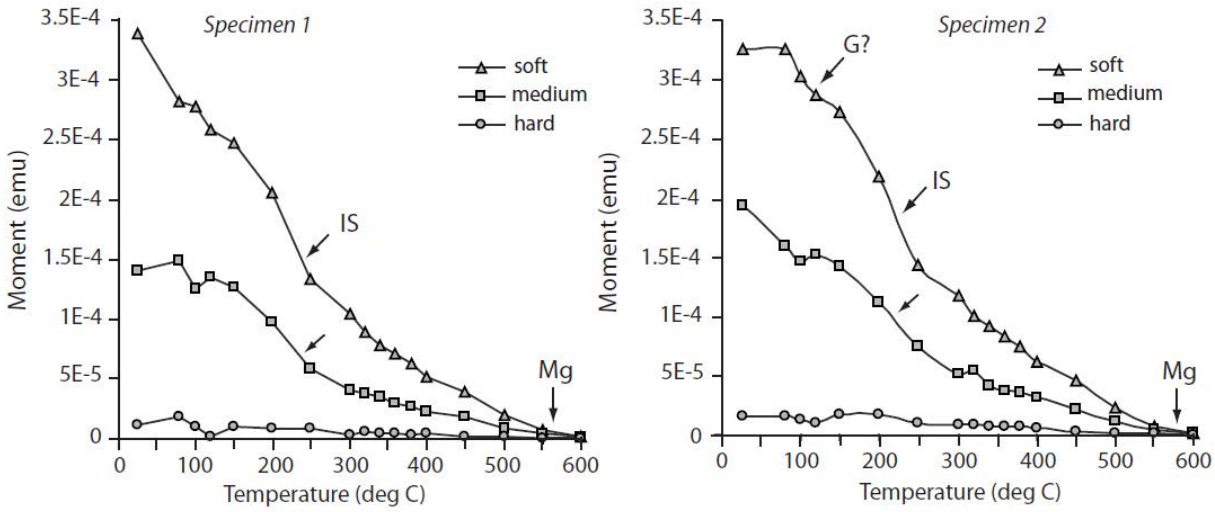

778

779 Figure 3

780

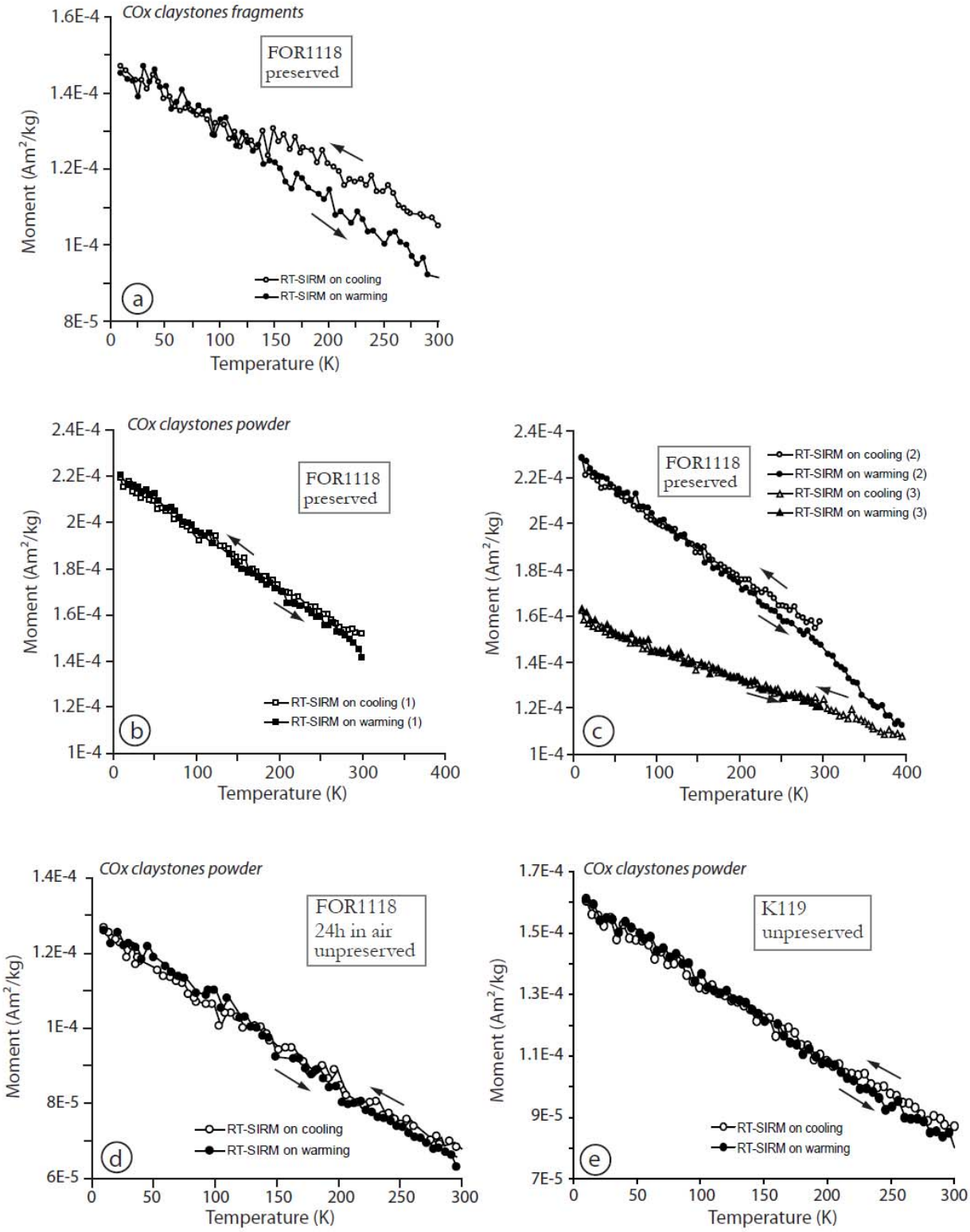

781

782 Figure 4

783

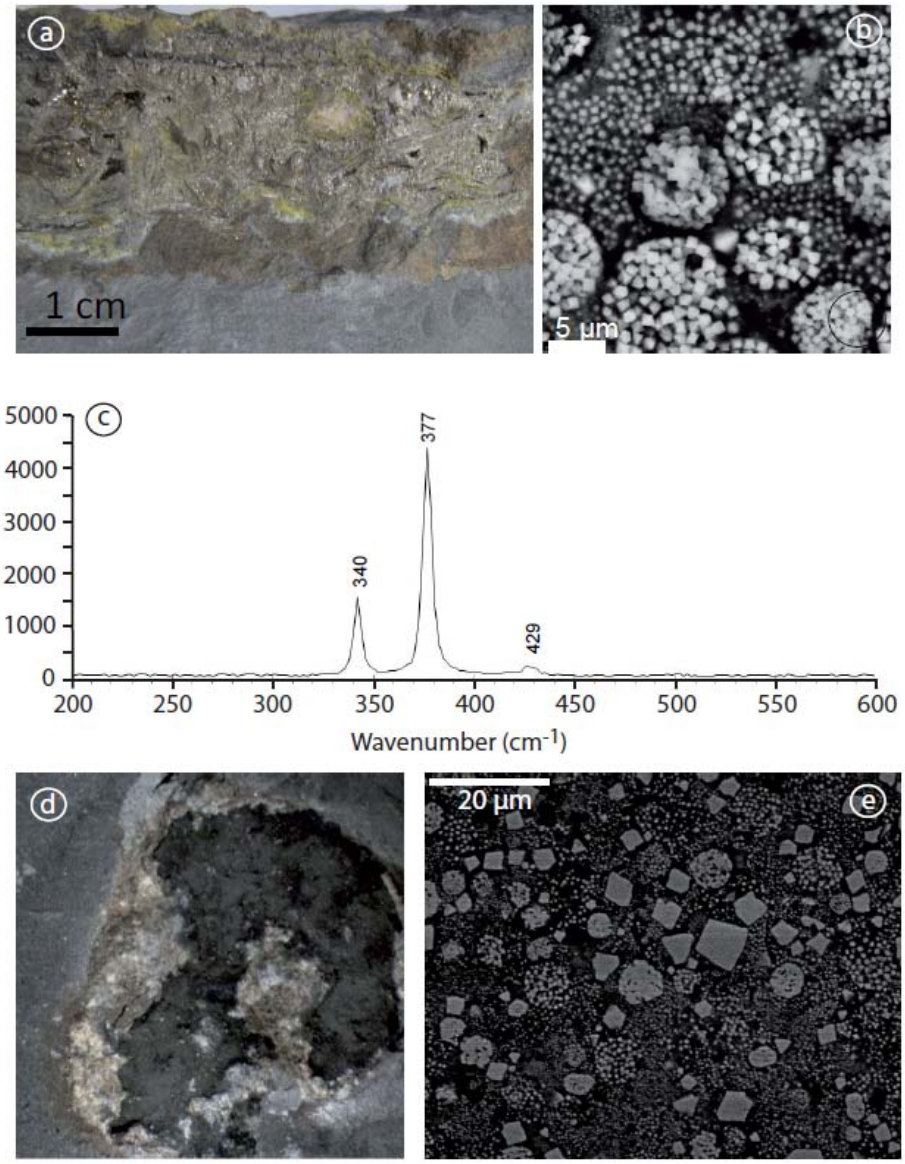

784

785 Figure 5

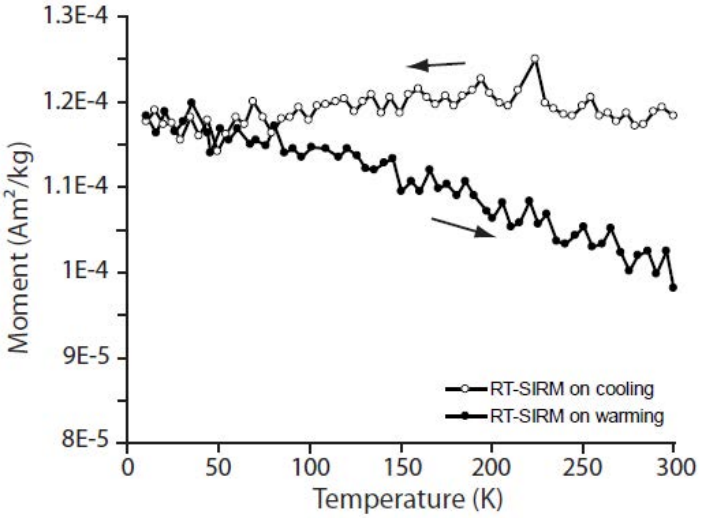

786

787 Figure 6

788

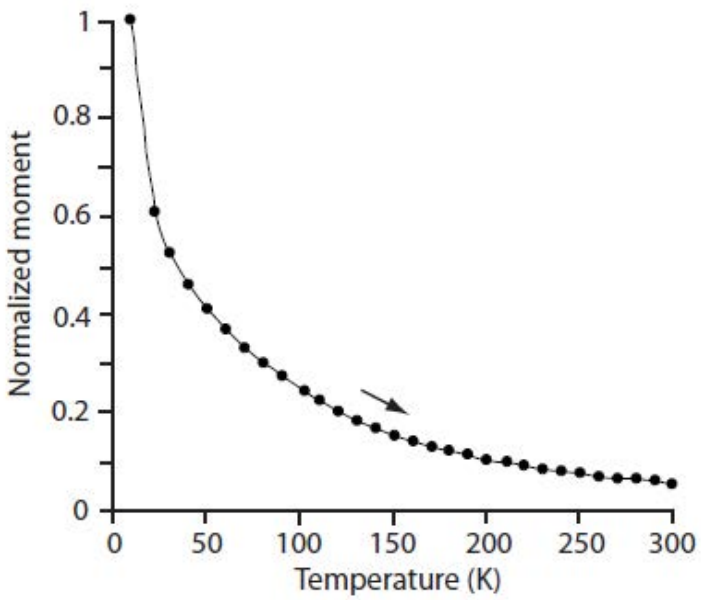

789

790 Figure 7

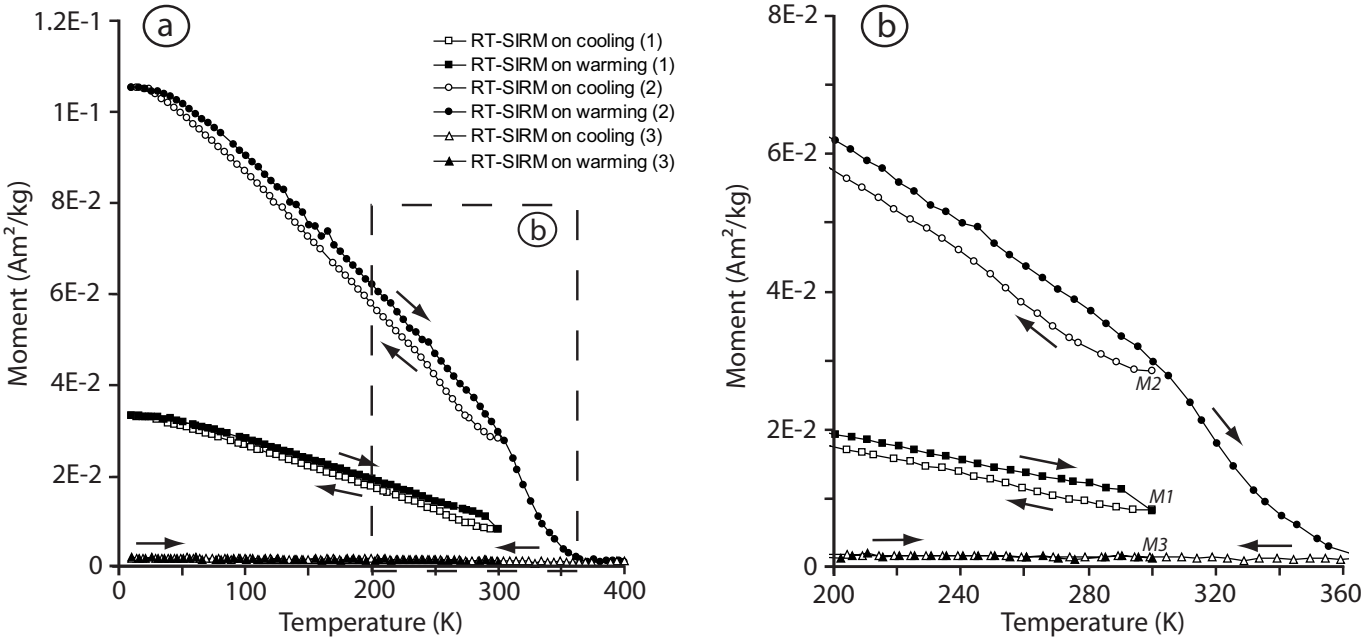
a
b
RT-SIRM on cooling (1)
RT-SIRM on warming (1)
RT-SIRM on cooling (2)
RT-SIRM on warming (2)
RT-SIRM on cooling (3)
RT-SIRM on warming (3)
Moment (Am²/kg)
Temperature (K)
1.2E-1
1E-1
8E-2
6E-2
4E-2
2E-2
0
100
200
300
400
M1
M2
M3
240
280
320
360

Figure 1

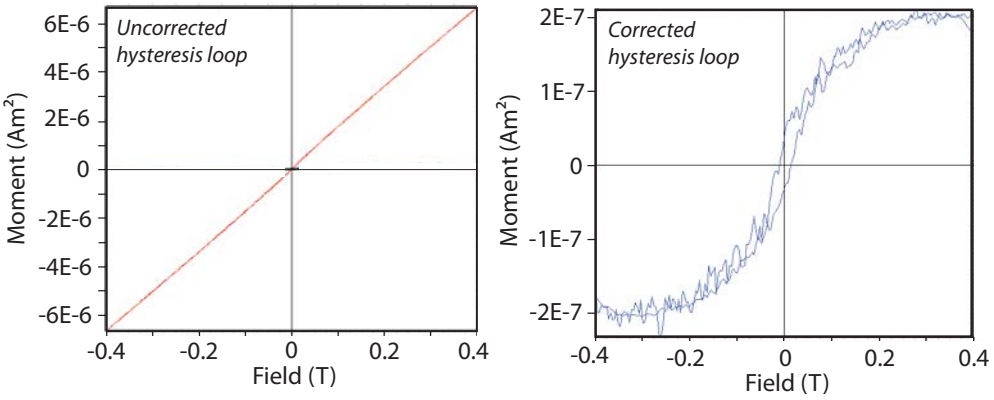
Uncorrected
hysteresis loop
Moment (Am²)
6E-6
4E-6
2E-6
0
-2E-6
-4E-6
-6E-6
-0.4
-0.2
0
0.2
0.4
Field (T)
Corrected
hysteresis loop
Moment (Am²)
2E-7
1E-7
0
-1E-7
-2E-7
-0.4
-0.2
0
0.2
0.4
Field (T)

Figure 2

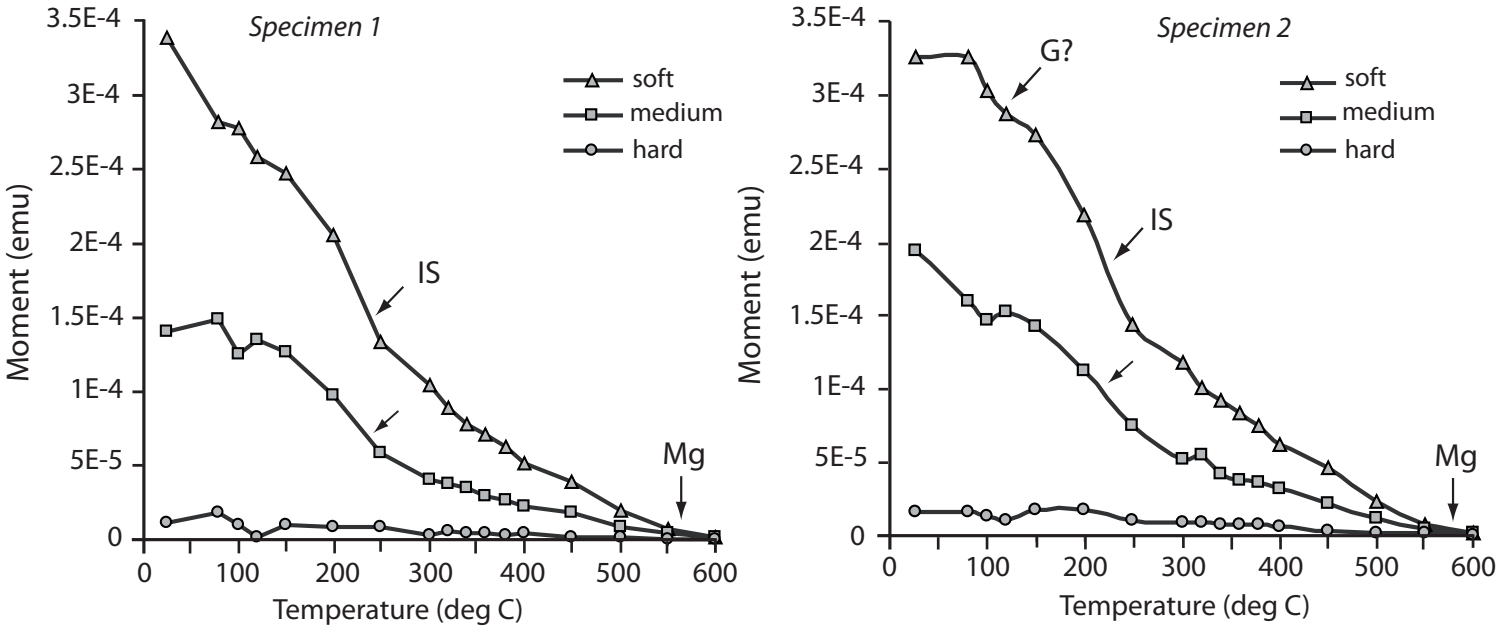
Specimen 1
soft
medium
hard
IS
Mg
Moment (emu)
Temperature (deg C)
3.5E-4
3E-4
2.5E-4
2E-4
1.5E-4
1E-4
5E-5
0
0
100
200
300
400
500
600
Specimen 2
G?
IS
Mg
soft
medium
hard
Moment (emu)
Temperature (deg C)

Figure 3

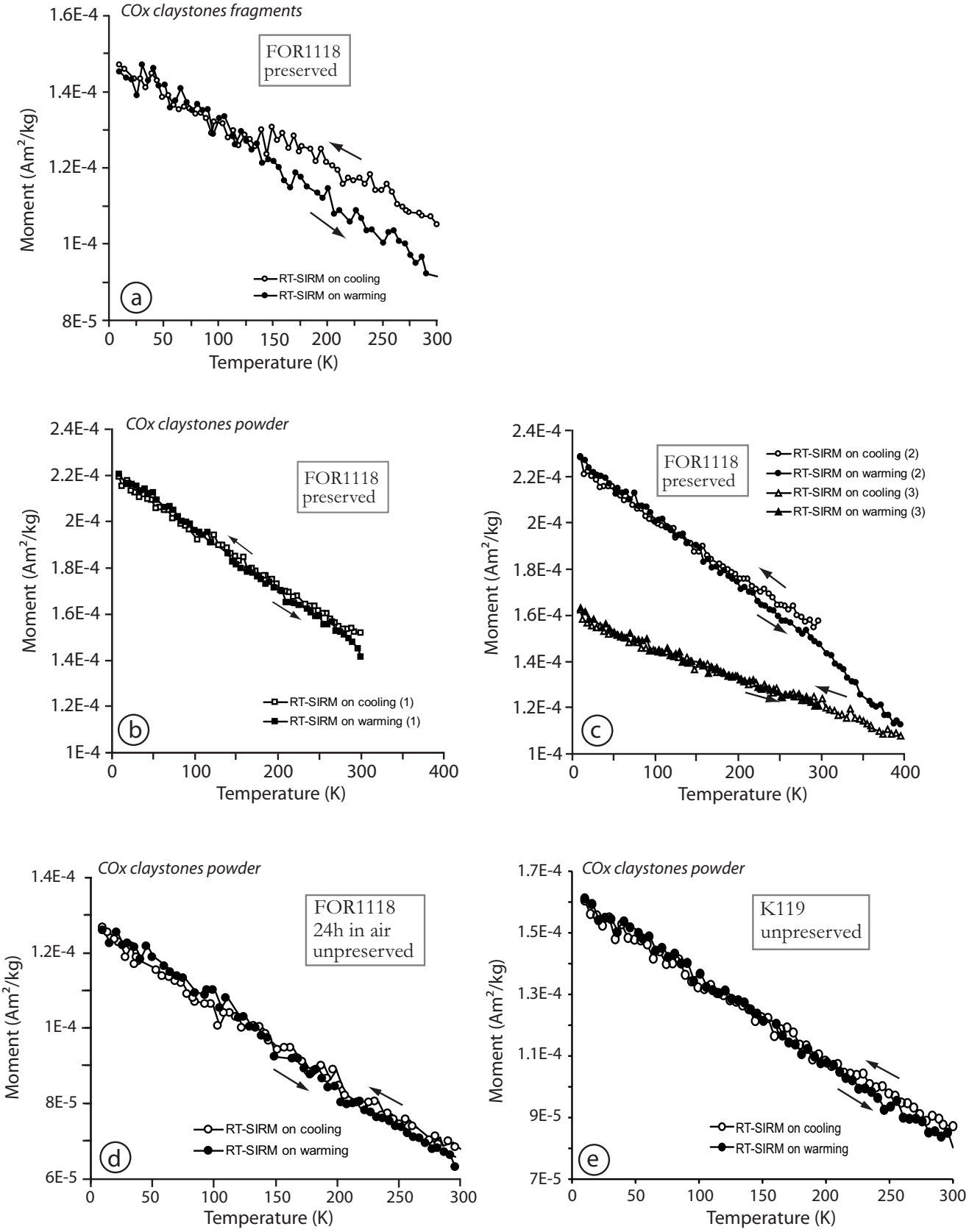
COx claystones fragments
FOR1118
preserved
RT-SIRM on cooling
RT-SIRM on warming
a
Moment (Am²/kg)
Temperature (K)
COx claystones powder
FOR1118
preserved
RT-SIRM on cooling (1)
RT-SIRM on warming (1)
b
COx claystones powder
FOR1118
preserved
RT-SIRM on cooling (2)
RT-SIRM on warming (2)
RT-SIRM on cooling (3)
RT-SIRM on warming (3)
c
COx claystones powder
FOR1118
24h in air
unpreserved
RT-SIRM on cooling
RT-SIRM on warming
d
COx claystones powder
K119
unpreserved
RT-SIRM on cooling
RT-SIRM on warming
e

Figure 4

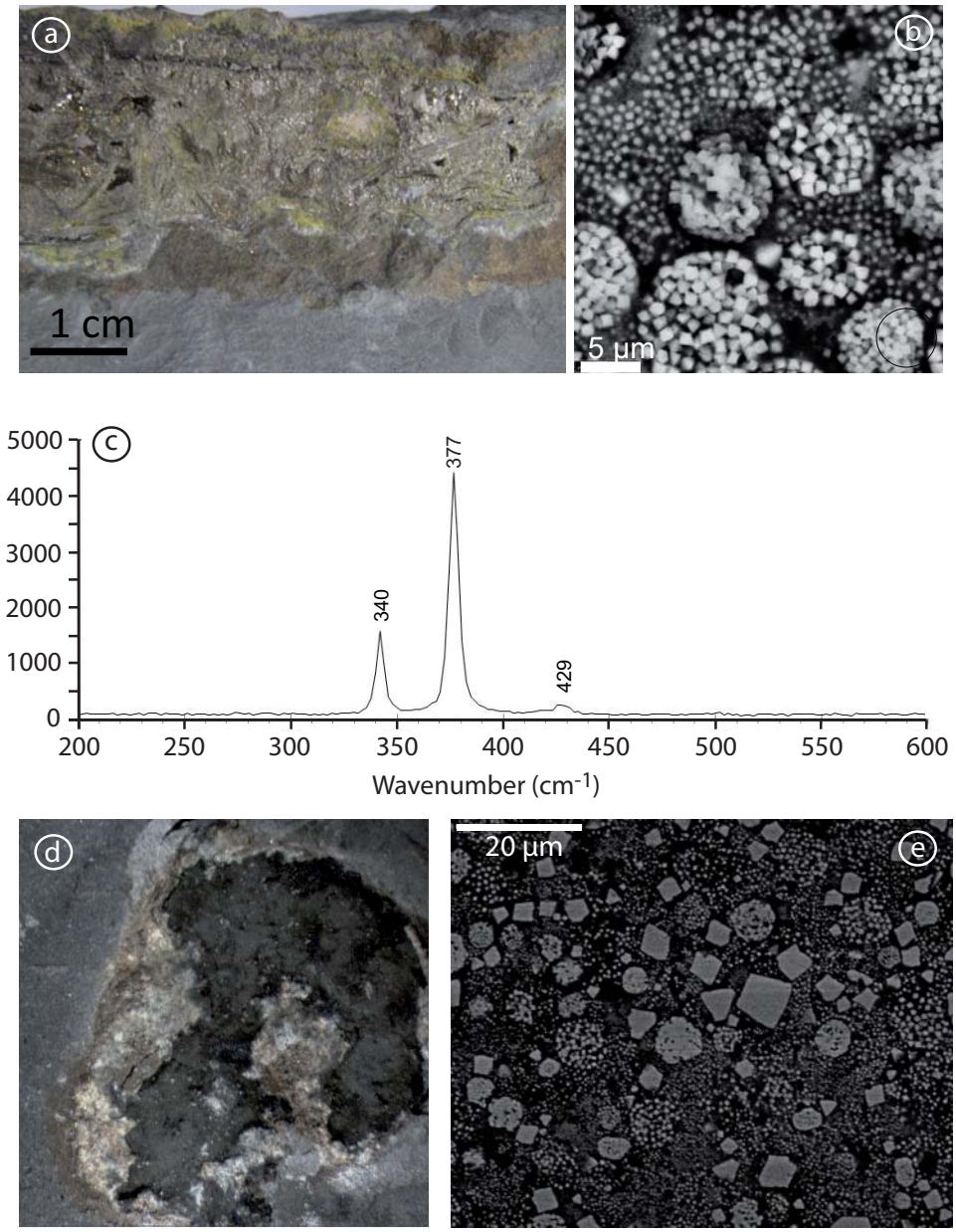
a
1 cm
b
5 µm
c
5000
4000
3000
2000
1000
0
340
377
429
200
250
300
350
400
450
500
550
600
Wavenumber (cm-1)
d
20 µm
e

Figure 5

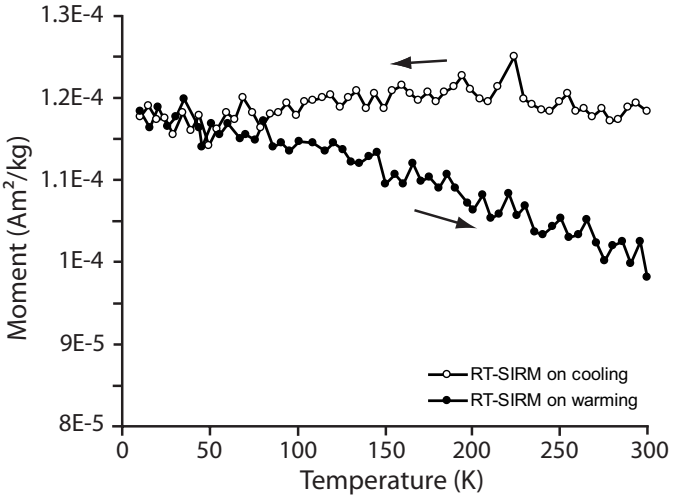
1.3E-4
1.2E-4
1.1E-4
1E-4
9E-5
8E-5
Moment (Am²/kg)
0
50
100
150
200
250
300
Temperature (K)
RT-SIRM on cooling
RT-SIRM on warming

Figure 6

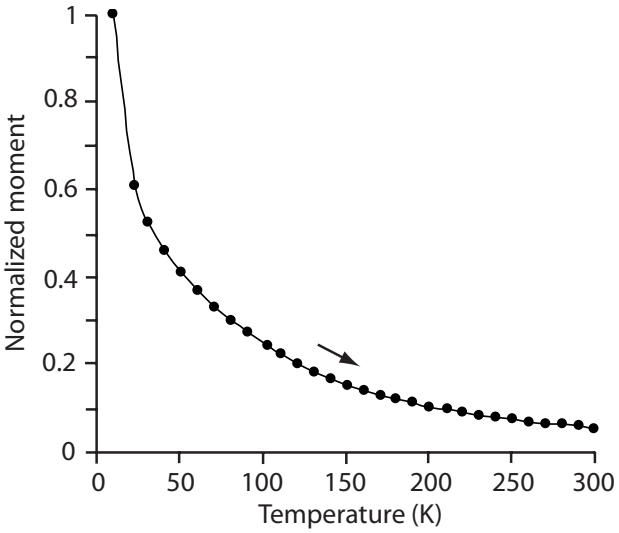
Normalized moment
1
0.8
0.6
0.4
0.2
0
0
50
100
150
200
250
300
Temperature (K)

Figure 7